IMPERIAL

**ME4 INDIVIDUAL PROJECT**

**FINAL REPORT**

# 1D NUMERICAL MODELLING FOR LITHIUM-SULFUR BATTERIES

Name: Dharshannan Sugunan

Supervisor(s): Dr. Monica Marinescu, Dr. Michael Cornish

Date: 05/06/2024

Number of pages: 40

Department of Mechanical Engineering,

Imperial College London

# ABSTRACT

This report focuses on the development of a novel solver for lithium-sulfur (Li-S) battery modeling, tailored for 0D models and optimized for the complexity of spatial resolution in 1D models adapted from literature. The solver was tested both with and without precipitation/dissolution dynamics, revealing key insights into the system's behavior. Initial discrepancies in the boundary conditions were rectified, leading to more accurate and stable results when these dynamics were included. Extensive tests on mass and charge conservation as well as cathode partial currents and species concentrations validated the solver's accuracy, although some discrepancies were observed during the high-to-low plateau transition due to model simplifications. Consecutive charge tests highlighted numerical stability issues related to $Li_2S_{(s)}$ solubility constants, reflecting challenges seen in previous research. Overall, the novel solver represents a significant advancement, addressing limitations of earlier models and enhancing the precision and reliability of Li-S battery simulations. This work refines numerical methods and improves understanding of complex behaviors within Li-S batteries, building on and enhancing previous research in the field.

# TABLE OF CONTENTS

# 1) INTRODUCTION

## 1.1) BACKGROUND INFORMATION

Research into lithium-sulfur (Li-S) batteries has surged alongside the expansion of electric transportation, driven by the quest for chemistries with higher energy density and the elimination of expensive, scarce, or unreliable materials from the battery supply chain. Projections suggest that lithium-sulfur batteries could offer roughly three times the energy density of lithium-ion batteries (1). The utilization of sulfur as a cathode material holds significant promise due to its affordability and widespread availability, crucial factors influencing both cost and the stability of the supply chain. Despite their potential, numerous obstacles have impeded the commercialization of these batteries such as polysulfide shuttling effects, capacity fade and low Coulombic efficiency.

In order to address and overcome these impediments and fully harness the potential of Li-S batteries, it is imperative to employ numerical modeling techniques. In this regard, PyBaMM (2), an open-source Python library utilizing the Casadi solver for differential algebraic equation (DAE) simulations, has gained recognition among researchers in the battery and energy storage domain. However, it is worth noting that the stability of this DAE solver is limited, particularly in the context of the most recent Li-S battery models. This limitation may compel some researchers to favor the use of data-driven models trained via machine learning techniques, owing to their numerical robustness, even though these models may lack the valuable insights inherent to physics-based models. COMSOL Multiphysics is another widely recognized modelling software used in modelling battery chemistries. However, its "black-box" nature, which makes it difficult for end users to access the solver class and adjust key solver hyper-parameters, poses challenges when debugging numerical issues and instabilities within implemented models.

## 1.2) PROJECT OBJECTIVES

The overall objective of this Final Year Project (FYP) is to enhance an existing innovative novel solver tailored for reduced-order (0D) Lithium-Sulfur (Li-S) simulation coded on Python (3) and successfully tested on models by Marinescu et al. (4) and Cornish et al. (5). This project endeavors to advance the said solver by leveraging its optimized numerical methodologies to simulate the performance of more complex higher-order (spatially resolved) Li-S battery models. The objectives of this project are summarized as below:

- Re-vamp existing 0D Li-S solver to incorporate complex operations of higher order models.
- Implement a 1D Li-S cell model adapted from Kumaresan et al. (6) and Zhang et al. (7) in Python and carry out testing of model stability.
- Optimize solver hyper-parameters and test reformulation of model equations based on stability analysis of the implemented 1D model.
- Carry out error analysis on simulated results in aspects of mass and charge conservation of the implemented 1D Li-S model and investigate cell voltage and current responses.
- Validate capability of finalized 1D Li-S solver and model by subjecting it to Galvanostatic Intermittent Titration Technique (GITT) and non-constant current analysis.

The overall structure of this report will follow the objectives as above. This will include formulations of the 1D Li-S model implemented in the Methodology section, integral quantities plots (voltage, partial currents, & species concentrations), error analysis (mass conservation & charge conservation) of these quantities and validation tests in the Results and Discussion section. The results obtained will be studied further and compared with those obtained from other authors.

# 2) LITERATURE REVIEW

## 2.1) Li-S MODELLING APPROACHES

The Li-S domain in most modelling approaches is represented as 3 regions, the Li metal anode, a porous separator and composite cathode.

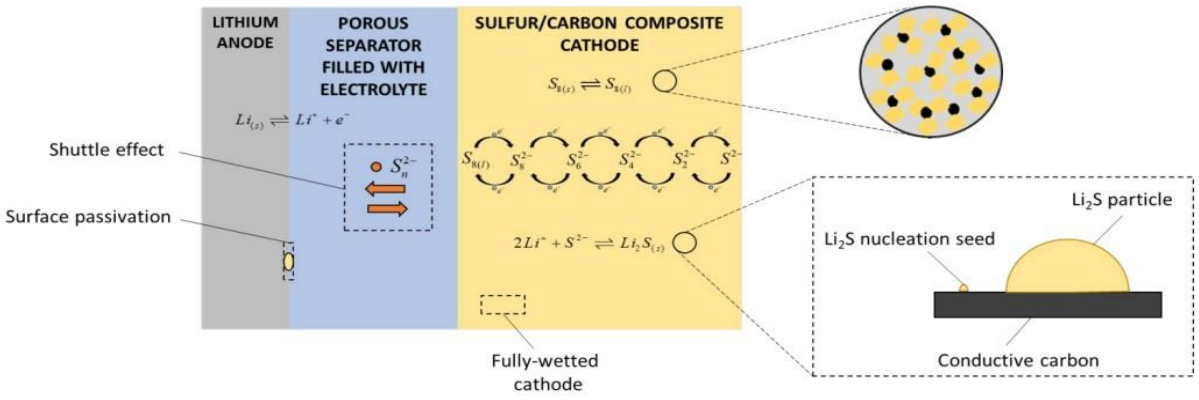


Figure 1. Li-S cell domain used in numerical modelling adapted from (1).

For a cell that is fully charged, the cathode is composed of solid sulfur, $S_{8(s)}$, and carbon nanotubes. In discharge, the $S_{8(s)}$ dissolves and is converted to lower order polysulfide species via a cascade of electrochemical reactions. Most of the higher order polysulfide species are soluble in the electrolyte of the cell, while the lower order polysulfides tend to precipitate in the cathode forming insulating $Li_2S$ as an insoluble product which leads to the surface passivation of the carbon structure towards the end of discharge as explained by Mistry and Mukherjee (8). During discharge or charge, polysulfides form at the cathode and dissolve into the electrolyte. Driven by a concentration gradient, these polysulfides diffuse towards the anode, where they can be reduced parasitically. Upon charging, they can migrate back to the cathode, creating a cyclic migration known as the "shuttle effect," which degrades battery performance. Hence, the reactions at the cathode are a key factor in capturing these electrochemical mechanisms within simulations. The two commonly employed reduction reactions at the cathode are the 2-stage reaction, which was developed by the works of Mikhaylik and Akridge (9) given as below:

$$S_{8(l)} + 4e^- \rightarrow 2S_4^{2-}$$

$$S_4^{2-} + 4e^- \rightarrow 2S^{2-} + S_2^{2-}$$

The other is the 5-stage reaction described in Figure 2 which is also used in a 1D model proposed by Kumaresan et al. (6).

## 2.2) 0D VS 1D Li-S CELL MODELS

The two prominent types of physics-based models implemented for Li-S simulations are the 0D and 1D models. 0D models generally only model the cathode as a singular point in space and are more computationally efficient, however are incapable of capturing transport limitations as expressed in the works of Marinescu et al. (4). A 1D model is more computationally expensive to solve, but is capable of resolving the transport limitations as evident from the well-studied Li-S model developed by Kumaresan et al. (6) which allows for a detailed analysis of the interplay between the mechanisms such as diffusion, precipitation/dissolution and electrochemistry.

Apart from computational limitations, 1D Li-S models also suffer from numerical instabilities which are far more prominent than 0D models. The studies from Ghaznavi & Chen (10) show significant instabilities when carrying out consecutive charge simulations (starting from the end-point of discharge) employing the Kumaresan model. These instabilities were attributed to the solubility constant of $Li_2S$ ($K_{Li_2S}$). This is an important test as it is also used as a validation test for the bespoke solver developed in this project which employs the modified model formulation proposed by Zhang (7). 0D models, however, show considerable numerical stability through multiple cycles of discharge and charge as is evident from the findings of Marinescu et al. (11).

Another key difference between the 1D model proposed by Kumaresan and the 0D models used by Marinescu (4,11), is the absence of shuttling effects in the 1D model. However, the 1D models suggested by Hofmann et al. (12) (2-stage) and Yoo et al. (13) (5-stage) both include the formulation of shuttling.

## 2.3) KUMARESAN MODEL: BASIS FOR 1D Li-S NOVEL SOLVER DEVELOPMENT

In this project, the Kumaresan 1D Li-S model was used as the basis to validate and test the development of the bespoke solver despite the absence of the significant shuttling process. This was done to ensure the simplicity of the already complex implementation of the model formulation and to ease the process of debugging during development. Nevertheless, the aim of this FYP is to develop an independent solver not limited to a single model, and the finalized version of said solver may be used to simulate 1D models with shuttling implemented such as Hofmann and Yoo (12,13) in future works. Further simplifying the model, the proposed formulation from Zhang et al. (7) is adopted which only accounts for the precipitation of $Li_2S$ species without precipitation of higher order polysulfides ($Li_2S_8$ , $Li_2S_4$ & $Li_2S_2$) as proposed by Kumaresan since $Li_2S$ is the only experimentally detected solid discharge product in Li-S cells.

To further test and validate the solver capabilities the tests proposed by Ghaznavi & Chen in (10,14,15) are used to observe the cathode partial currents profile, effects of precipitation constants and the problems encountered in consecutive charge of the model.

## 2.4) LITERATURE REVIEW SUMMARY

This section outlines various modeling approaches for lithium-sulfur (Li-S) batteries, focusing on the representation of the Li-S domain and the cathode reactions. The two main modeling frameworks discussed are 0D and 1D models, each with their computational advantages and limitations. The 1D model proposed by Kumaresan serves as the basis for the development of a novel solver in this project, despite its omission of significant shuttling effects and numerical instabilities during charge. Additionally, the solver's formulation is simplified based on Zhang et al.'s (7) work, focusing solely on the precipitation of $Li_2S$ species to align with experimental observations. Various validation tests are proposed to assess the solver's capabilities based on the works of Ghaznavi & Chen (10,14,15).

# 3) METHODOLOGY

## 3.1) COMPUTATIONAL DOMAIN AND UNDERLYING EQUATIONS

The domain for the 1D Li-S model adapted from figure 1 is given as below in figure 2 with the boundary conditions used:

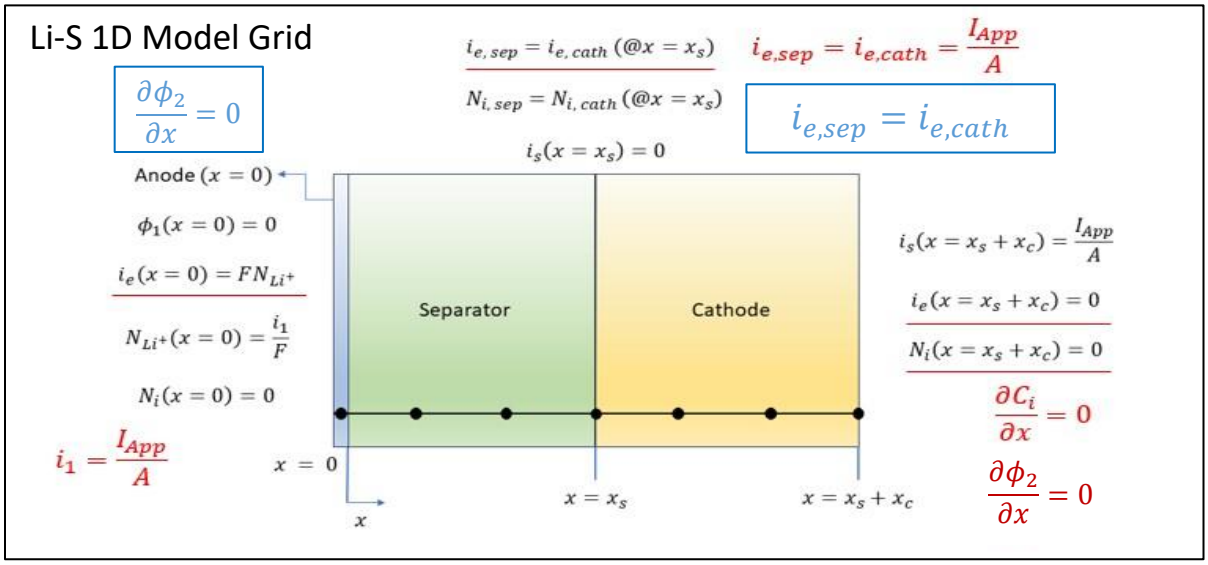


Figure 2. Computational domain and boundary conditions.

The domain is divided into 2 regions, the separator and cathode, with 3 boundaries, the anode/separator interface, separator/cathode interface and the cathode current collector. Each boundary has its own prescribed boundary conditions as depicted in figure 2 above. The boundary equations underlined in red are further investigated and modified with the equations in red and blue (section 4.3). The overall boundary conditions given are adapted from Kumaresan. Further testing results of the modified boundary conditions are provided in the Results and Discussion section 4.3. The 1D Kumaresan model is characterized as a 6-stage reaction, with lithium chemistry in the anode followed by a 5-stage cascade reaction of polysulfide species in the cathode. The chemical equations are given as below:

$$Li \leftrightarrow Li^+ + e^- \qquad [1]$$

$$\frac{1}{2}S_{8(l)} + e^- \leftrightarrow \frac{1}{2}S_8^{2-} \quad [2]$$

$$\frac{3}{2}S_8^{2-} + e^- \leftrightarrow 2S_6^{2-} \quad [3]$$

$$S_6^{2-} + e^- \leftrightarrow \frac{3}{2}S_4^{2-} \quad [4]$$

$$\frac{1}{2}S_4^{2-} + e^- \leftrightarrow S_2^{2-} \quad [5]$$

$$\frac{1}{2}S_2^{2-} + e^- \leftrightarrow S^{2-} \quad [6]$$

The simplification to precipitation and dissolution dynamics as mentioned before is adopted from Zhang (7) which only accounts for the precipitation of $Li_2S_{(s)}$ species and dissolution of $S_{8(s)}$. The overall governing equations of the 1D Li-S model are provided as follows.

The continuity equation of concentration of species $C_i$, is given such, with $\epsilon$ being the pore volume fraction, $N_i$ is flux, $r_i$ is the rate of electrochemical reactions and $R_i$ is rate of precipitation/dissolution of species $i$ ($i = Li^+, S_8, S_8^{2-}, S_6^{2-}, S_4^{2-}, S_2^{2-}, S^{2-}, A^-$):

$$\frac{\partial(\epsilon C_i)}{\partial t} = -\nabla . N_i + r_i - R_i \quad [7]$$

The flux, $N_i$, is given as follows, where $D_i^{eff}$ is the effective diffusion coefficient, $z_i$ is the charge number, *R* gas constant, *T* temperature, *F* faradays constant, and $\phi_2$ electrolyte potential:

$$N_i = -D_i^{eff}\nabla C_i - \frac{z_i D_i^{eff}}{RT} F C_i \nabla \phi_2 \quad [8]$$

The electrochemical rate of reaction, with $n_j$ being the number of $e^-$ transferred in reaction *j*, $s_{i,j}$ the stoichiometric coefficient of species *i* in reaction *j*, $i_j$ the current density of reaction *j*, and $a_v$ the specific area of cathode:

$$r_i = a_v \sum_j \frac{s_{i,j} i_j}{n_j F} \quad [9]$$

The precipitation/dissolution rate, $R_i$ is given with, $R'_k$ the rate of precipitation of solid species *k* ($k = S_{8(s)}, Li_2S_{(s)}$), and $\gamma_{i,k}$ the number of moles of species *i* in solid *k*:

$$R_i = \sum_k \gamma_{i,k} R'_k \quad [10]$$

The governing equations are constrained to obey the current continuity equation for which $i_e$ is the electrolyte current and $i_s$ is the solid-state current:

$$\nabla . i_e + \nabla . i_s = 0 \quad [11]$$

$$i_e = F \sum_i z_i N_i \, , i_s = -\sigma \nabla \phi_1 \quad [12]$$

$$\nabla . i_e = a_v \sum_j i_j \quad [13]$$

Where, $\sigma$ is the solid-state conductivity and $\phi_1$ solid-state potential. Equation [13] is another constraint on the electrolyte current with respect to the cathode partial currents.

The change in pore volume fraction, $\epsilon$ of cathode/separator and the pore volume fractions of species *k* due to precipitation/dissolution, $\epsilon_k$ is given as, with $\widetilde{V_k}$, molar volume of species *k*:

$$\frac{\partial \epsilon}{\partial t} = -\sum_k \widetilde{V_k} R'_k \quad [14]$$

$$\frac{\partial \epsilon_k}{\partial t} = \widetilde{V_k} R'_k \quad [15]$$

The Butler-Volmer current density equation, with $i_{0,j}$ the exchange current density of reaction *j*, $C_{i,ref}$ the initial species concentration, and $p_{i,j} = s_{i,j}$ for oxidized species and $q_{i,j} = -s_{i,j}$ for reduced species, is given as below:

$$i_j = i_{0,j} \left\{ \prod_i \left( \frac{C_i}{C_{i,ref}} \right)^{p_{i,j}} e^{\frac{0.5F}{RT}\eta_j} - \prod_i \left( \frac{C_i}{C_{i,ref}} \right)^{q_{i,j}} e^{-\frac{0.5F}{RT}\eta_j} \right\} \quad [16]$$

The remaining underlying expressions are given as such:

$$\eta_j = \phi_1 - \phi_2 - U_{j,ref} \quad [17]$$

$$U_{j,ref} = U_j^{\theta} - \frac{RT}{n_j F}\sum s_{i,j} \ln\left(\frac{C_{i,ref}}{10^3}\right) \quad [18]$$

$$R_k' = k_k \epsilon_k \left[\prod_i (C_i)^{\gamma_{i,k}} - K_{sp,k}\right] \quad [19]$$

$$D_i^{eff} = D_i(\epsilon)^{1.5} \quad [20]$$

$$a_v = a_0\left(\frac{\epsilon}{\epsilon_{initial}}\right)^{1.5} \quad [21]$$

Where, $U_j^{\theta}$ is the standard equilibrium potential, $k_k$ & $K_{sp,k}$ the precipitation/dissolution rate constant and solubility of species *k* respectively, $D_i$ the bulk diffusion constant and $a_0$ the initial specific surface area of cathode.

## 3.2) EQUATIONS DISCRETISATION AND JACOBIAN MATRIX FORMULATION

The governing equations provided above are discretised temporally using the implicit Backwards Euler scheme. An implicit scheme is chosen owing to its stability as opposed to an explicit scheme for which the solution diverges rapidly for a stiff system of equations. The Backwards Euler scheme is used due to its simplicity in discretization, despite its 1st order accuracy. The general Backwards Euler scheme is given as follows:

$$\left.\frac{df}{dt}\right|_{n+1} = \frac{f_{n+1} - f_n}{\delta t} \quad [22]$$

For example, applying the discretization scheme to the time-dependent PDE governing the species concentrations, yields the following:

$$\frac{\partial D_i^{eff}}{\partial x} = 1.5 D_i \sqrt{\epsilon_p^{m,n+1}}\left[\frac{\epsilon_p^{m+1,n+1} - \epsilon_p^{m,n+1}}{\delta x}\right] \quad [23]$$

$$D_i^{eff} = D_i\left(\epsilon_p^{m,n+1}\right)^{1.5} \quad [24]$$

$$\nabla . N_i = -\left[\frac{D_i^{eff}\left(C_i^{m+1,n+1} - 2C_i^{m,n+1} + C_i^{m-1,n+1}\right)}{\delta x^2} + \left(\frac{C_i^{m+1,n+1} - C_i^{m,n+1}}{\delta x}\right)\left(\frac{\partial D_i^{eff}}{\partial x}\right)\right] \quad [25]$$

$$-\frac{z_i F}{RT}\left[D_i^{eff} C_i^{m,n+1}\left(\frac{\phi_2^{m+1,n+1} - 2\phi_2^{m,n+1} + \phi_2^{m-1,n+1}}{\delta x^2}\right)\right.$$

$$+ D_i^{eff}\left(\frac{C_i^{m+1,n+1} - C_i^{m,n+1}}{\delta x}\right)\left(\frac{\phi_2^{m+1,n+1} - \phi_2^{m,n+1}}{\delta x}\right)$$

$$\left. + C_i^{m,n+1}\left(\frac{\partial D_i^{eff}}{\partial x}\right)\left(\frac{\phi_2^{m+1,n+1} - \phi_2^{m,n+1}}{\delta x}\right)\right]$$

$$\frac{\partial(\epsilon C_i)}{\partial t} = \epsilon_p^{m,n+1}\left(\frac{C_i^{m,n+1} - C_i^{m,n}}{\delta t}\right) + C_i^{m,n+1}\left(\frac{\epsilon_p^{m,n+1} - \epsilon_p^{m,n}}{\delta t}\right) = -\nabla . N_i + r_i - R_i \quad [26]$$

The $m, n$ terms represent spatial and temporal discretization respectively, while for $\epsilon_p$, the *p* represents the different pore volume fractions in the cathode and separator ($p = cath\ or\ sep$). The $r_i$ & $R_i$ terms are also discretized in terms of the species at the current spatial position and next time step $(m, n+1)$.

The other equations (precipitation/dissolution) are discretized in a similar fashion (not-provided here to reduce the amount of mathematical complexity). The boundary conditions are also discretized similarly, for example the zero potential gradient and concentration gradients at the cathode current collector boundary is formulated as below:

$$\left.\frac{\partial \phi_2}{\partial x}\right|_{x=x_s+x_c} = \frac{\phi_2^{m,n+1} - \phi_2^{m-1,n+1}}{\delta x} = 0 \quad [27]$$

At the cathode boundary, a backward spatial differential is used to account for non-existent spatial nodes on the right-hand side of the boundary and for the anode boundary a forward spatial differential is used to account for non-existent spatial nodes on the left-hand side, such as:

$$\left.\frac{\partial \phi_2}{\partial x}\right|_{x=0} = \frac{\phi_2^{m+1,n+1} - \phi_2^{m,n+1}}{\delta x} = 0 \quad [28]$$

The system of discretized equations is solved employing a Newton-Raphson approach, which is a commonly employed method for non-linear set of ODEs and PDEs. The matrix representation of the Newton-Raphson method is as follows:

$$\boldsymbol{x}_{k+1} = \boldsymbol{x}_k - \alpha \boldsymbol{J}^{-1}\boldsymbol{F} \quad [30]$$

Where, $\boldsymbol{x}_k$ & $\boldsymbol{x}_{k+1}$ are the current and next variable vectors, $\boldsymbol{J}$ & $\boldsymbol{F}$ are the Jacobian matrix and residual vector respectively. The residual vector, $\boldsymbol{F}$ is obtained using the discretized equations, by re-arranging all terms of the equation to one side so that the equation equals zero. These equations which equate to zero, are now called the residual functions. The formulation of the Jacobian matrix, $\boldsymbol{J}$, however, is more complex. A simple demonstration of how the matrix is formed for 2 boundary points and 1 internal point with 2 variables ($S_8$ & $S_8^{2-}$) is provided as follows. Note the variable vector is provided only for sequence visualization purposes next to the Jacobian matrix, where $x_0$ & $(x_2 = x_L)$ are the boundary points while $x_1$ is the internal point.

$$\begin{pmatrix} \frac{\partial u_{B1,x_0}}{\partial S_8|_{x_0}} & \frac{\partial u_{B1,x_0}}{\partial S_8|_{x_1}} & 0 & 0 & 0 & 0 \\ \frac{\partial u_1}{\partial S_8|_{x_0}} & \frac{\partial u_1}{\partial S_8|_{x_1}} & \frac{\partial u_1}{\partial S_8|_{x_2}} & 0 & \frac{\partial u_1}{\partial S_8^{2-}|_{x_1}} & 0 \\ 0 & \frac{\partial u_{B1,x_L}}{\partial S_8|_{x_1}} & \frac{\partial u_{B1,x_L}}{\partial S_8|_{x_2}} & 0 & 0 & 0 \\ 0 & 0 & 0 & \frac{\partial u_{B2,x_0}}{\partial S_8^{2-}|_{x_0}} & \frac{\partial u_{B2,x_0}}{\partial S_8^{2-}|_{x_1}} & 0 \\ 0 & \frac{\partial u_2}{\partial S_8|_{x_1}} & 0 & \frac{\partial u_2}{\partial S_8^{2-}|_{x_0}} & \frac{\partial u_2}{\partial S_8^{2-}|_{x_1}} & \frac{\partial u_2}{\partial S_8^{2-}|_{x_2}} \\ 0 & 0 & 0 & 0 & \frac{\partial u_{B2,x_L}}{\partial S_8^{2-}|_{x_1}} & \frac{\partial u_{B2,x_L}}{\partial S_8^{2-}|_{x_2}} \end{pmatrix} \begin{pmatrix} S_8|_{x_0} \\ S_8|_{x_1} \\ S_8|_{x_2} \\ S_8^{2-}|_{x_0} \\ S_8^{2-}|_{x_1} \\ S_8^{2-}|_{x_2} \end{pmatrix}$$

Table 1. Residual functions for example Jacobian matrix.

| Residual | Explanation | Dependent Variables |
|---|---|---|
| $u_{B1,x_0}$ | Residual for boundary condition of $S_8$ at $x_0$ | $f(S_8\|_{x_0}, S_8\|_{x_1})$ |

| | | |
|---|---|---|
| $u_{B1,x_L}$ | Residual for boundary condition of $S_8$ at $x_L$ | $f(S_8\|_{x_1}, S_8\|_{x_2})$ |
| $u_1$ | Residual for internal points of $S_8$ | $f(S_8\|_{x_0}, S_8\|_{x_1}, S_8\|_{x_2}, S_8^{2-}\|_{x_1})$ |
| $u_{B2,x_0}$ | Residual for boundary condition of $S_8^{2-}$ at $x_0$ | $f(S_8^{2-}\|_{x_0}, S_8^{2-}\|_{x_1})$ |
| $u_{B2,x_L}$ | Residual for boundary condition of $S_8^{2-}$ at $x_L$ | $f(S_8^{2-}\|_{x_1}, S_8^{2-}\|_{x_2})$ |
| $u_2$ | Residual for internal points of $S_8^{2-}$ | $f(S_8\|_{x_1}, S_8^{2-}\|_{x_0}, S_8^{2-}\|_{x_1}, S_8^{2-}\|_{x_2})$ |

Each element of the Jacobian matrix is formed using the partial derivatives of each residual function with respect to the dependent variables, for residuals that do not depend on a variable, that specific element will be set to zero. It is to be noted that due to the existence of different pore volume fractions for cathode and separator, the equation [26] which is used for the internal points of the variables will have 2 distinct sets of equations, one for the cathode and the other for the separator. The algorithm for the formation of the matrix is generalized within a Python script and the Jacobian formed is stored in memory as a symbolic matrix using the SymPy library. This symbolic matrix is then accessed at each time iteration of the solver to carry out variable substitution via a sequencing algorithm. The details on the matrix formulation algorithm and variable substitution will not be discussed further, however the GitHub repository link provided at the end of this report will include all the Python scripts used. The Jacobian is formed based on all the nodes and variables of the system, for example if there are 25 nodes (incl. boundary and internal points), and 16 variables, the total number of variables to be solved for is $25 \times 16 = 400$, thus the Jacobian will be a $(400 \times 400)$ matrix, which is mostly sparse.

## 3.3) SOLVER ALGORITHM

Due to the large sparse matrix, the solver which is coded in Python is optimized for efficient computations. This is achieved using 2 key numerical techniques, the modified Newton-Raphson (NR) approach and the adaptive-step size method. The modified NR method involves introducing a damping factor to the Jacobian matrix, $\alpha$ term in equation [30], which is dynamically updated to speed up computational time. The overall solver algorithm is depicted in the flow-chart below:

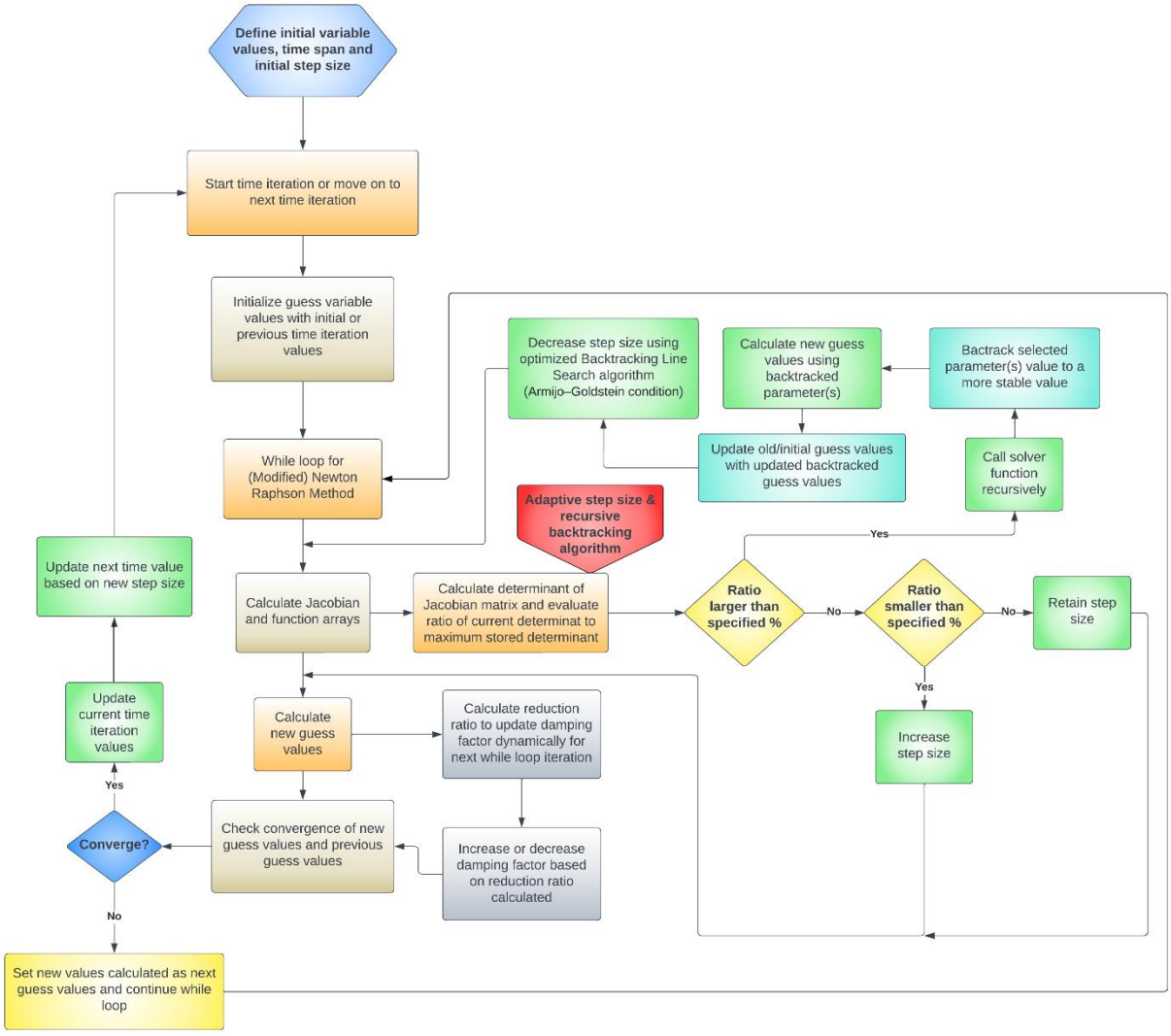


Figure 3. Solver algorithm flow-chart.

## 3.4) PENALTY METHOD

The last point to be explained for the system of equations formed, is the existence of domain specific variables. These variables such as the solid-state potential, $\phi_1$ are only present in a single domain, such as the cathode and not in the separator, similar for the pore volume fractions, $\epsilon_p$ which have individual values in the cathode and the separator. However, the Jacobian matrix formulation and variable substitution algorithms are coded such that all variables are assumed to exist in all domains. Hence, to address this issue and to remove the dependency of the solution obtained by the solver from these variables, the penalty method is used.

The penalty method involves adding a large factor, called a penalty factor to the diagonal term of the variable(s) in question. This addition of the penalty factor, effectively removes the influence of the variable on the system of equations, and the value of the variable remains unchanged throughout the simulation. For example, take the system of equations below:

$$\begin{pmatrix} k_{11}+C & k_{12} & k_{13} & k_{14} \\ k_{21} & k_{22}+C & k_{23} & k_{24} \\ k_{31} & k_{32} & k_{33} & k_{34} \\ k_{41} & k_{42} & k_{43} & k_{44} \end{pmatrix} \begin{pmatrix} x_1 \\ x_2 \\ x_3 \\ x_4 \end{pmatrix} = F$$

By the addition of the penalty factor *C*, to the diagonals $k_{11}$ & $k_{22}$, this removes the dependency of the solution from the $x_1$ & $x_2$ variables. This method is widely used in FEA programs (16) and is adopted here to address the problem faced in the 1D Li-S system of equations.

The method proves to be useful and works well, however, note that the magnitude of the penalty factor added to the Jacobian can severely impact the system of equations. If a factor that is too large is employed, the system becomes over-stiff and causes inaccuracies, while a factor that is too small will cause the unwanted variable(s) to still have an effect on the overall system. Hence, it is good practice to tune the penalty factor relative to the determinant of the Jacobian.

# 4) RESULTS AND DISCUSSION

## 4.1) INITIAL VALUE PROBLEM (ELECTROLYTE AND SOLID-STATE POTENTIALS)

The first hurdle faced when reviewing the parameters and initial conditions from both Kumaresan and Zhang is the initial conditions for $\phi_1$ and $\phi_2$ (solid state potential and electrolyte potential respectively) were not specifically mentioned. The initial conditions for the other species (i.e. $Li^+, S_{8,l},\ S_8^{2-}, S_6^{2-}, S_4^{2-}, S_2^{2-}, S^{2-}$ & $A^-$ ) where stated to be equal to their respective reference values ($C_i^{ref}$) and are assumed to be homogenous across the whole grid initially. Note that the $A^-$ species refers to the anion salt within the cell which does not take part in any electrochemical reactions, and is present only as a charge balance to the system.

Hence, to solve for the initial conditions of $\phi_1$ and $\phi_2$, a boundary value problem is formulated with the equations provided for electrolyte, $i_e$ and solid-state, $i_s$ currents. The $\phi_1$ residual is formulated using equation [11] and $\phi_2$ residual using equation [13], employing the relationships in equation [12]. The discretized residual functions are as below:

$\boldsymbol{\phi_1}$:

$$F\sum_i z_i\left\{-z_i\left(\frac{D_i^p F}{RT}\right)\left(\frac{C_i^{ref}\left[\phi_2^{m+1,n+1}-2\phi_2^{m,n+1}+\phi_2^{m-1,n+1}\right]}{\delta x^2}\right)\right\} \quad [31]$$

$$-\frac{\sigma\left[\phi_1^{m+1,n+1}-2\phi_1^{m,n+1}+\phi_1^{m-1,n+1}\right]}{\delta x^2}=0$$

$\boldsymbol{\phi_2}$:

$$F\sum_i z_i\left\{-z_i\left(\frac{D_i^p F}{RT}\right)\left(\frac{C_i^{ref}\left[\phi_2^{m+1,n+1}-2\phi_2^{m,n+1}+\phi_2^{m-1,n+1}\right]}{\delta x^2}\right)\right\}-a_V\sum_{j=2}^{6} i_j=0 \quad [32]$$

Note that for the sum of partial currents in equations [32] and all other discretized equations used, only $i_2 - i_6$ (polysulfide partial currents) are accounted for, this is due to the fact that $i_1$

represents the $Li$ reaction partial current which is only present in the anode (as a boundary condition) and not present in the cathode. Also note the following assumptions made for the initial value problem formulated:

- $\nabla C_i = \nabla^2 C_i = 0$, initial species concentrations constant & homogenous across grid.
- $D_i^p = D_i^{sep}$ $(0 < x < x_s)$, treated as a constant.
- $D_i^p = D_i^{cath}$ $(x_s < x < x_s + x_c)$, treated as a constant.
- $a_V \sum_j i_j = 0$ $(0 < x < x_s)$ , no electrochemical reactions in the separator region.
- $\sigma = 0$ $(0 < x < x_s)$ , $\sigma$ is effective conductivity of solid phase of the cathode, [S/m].

The boundary conditions for $\phi_1$ & $\phi_2$ are discretized similarly, using the original conditions provided in figure 2 (un-modified versions). The boundary condition formulations are as below:

1) $x = 0$:

$$\phi_1^{m,n+1}|_{x=0} = 0 \quad [33]$$

$$\phi_2^{m+1,n+1} - \phi_2^{m,n+1} + \frac{(i_1 RT)}{F^2 z_{Li} D_{Li}^{sep} C_{Li}} \delta x = 0 \quad [34]$$

2) $x = x_s$:

$$-\frac{\sigma\left(\phi_1^{m+1,n+1} - \phi_1^{m-1,n+1}\right)}{2\delta x} = 0 \quad [35]$$

$$\left\{ F \sum_i - \frac{z_i^2 \left(\frac{D_i^{sep}}{RT}\right) F C_i^{ref} \left[\phi_2^{m,n+1} - \phi_2^{m-1,n+1}\right]}{\delta x} \right\} \quad [36]$$

$$- \left\{ F \sum_i - \frac{z_i^2 \left(\frac{D_i^{cath}}{RT}\right) F C_i^{ref} \left[\phi_2^{m+1,n+1} - \phi_2^{m,n+1}\right]}{\delta x} \right\} = 0$$

3) $x = x_s + x_c$:

$$\phi_1^{m,n+1} - \phi_1^{m-1,n+1} + \frac{I_{App} \delta x}{\sigma A} = 0 \quad [37]$$

$$F\sum_i\left\{-\frac{z_i^2\left(\frac{D_i^{cath}}{RT}\right)FC_i^{ref}\left[\phi_2^{m,n+1}-\phi_2^{m-1,n+1}\right]}{\delta x}\right\}=0 \quad [38]$$

Where $A$ is the area of the cathode. The results obtained for the initial value problem, is depicted in figure 4 below, showing the initial distribution of the $\phi_1$ & $\phi_2$ potentials across the spatial domain of the cell, for different initial guess values:

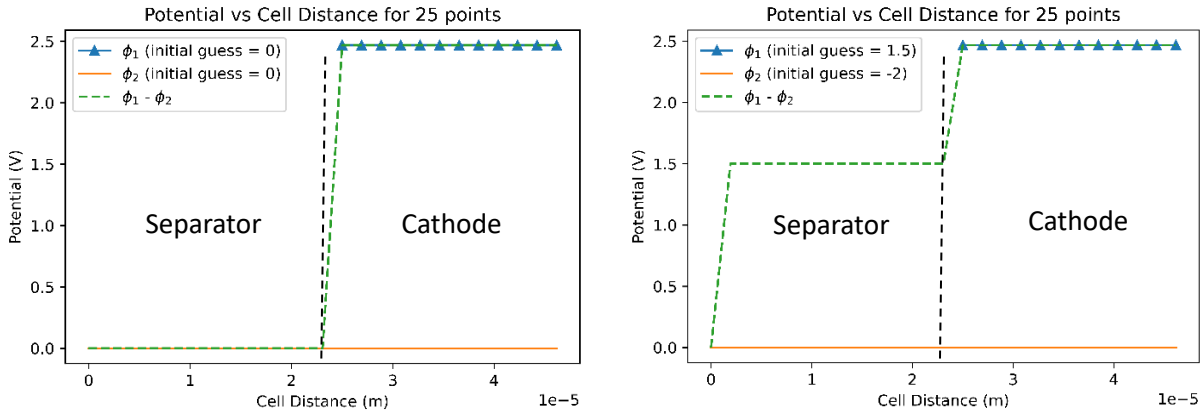


Figure 4. $\phi_1$ & $\phi_2$ potentials distributions.

It can be observed in figure 4 for any guess values of the initial potential conditions, the values always converge to the same results, for which $\phi_1 \approx U_2(2.41V)$ at the cathode and $\phi_2 = 0V$, where $U_2$ is the reference potential for reaction 2, given by equation [2]. The $\phi_1$ values in the separator remains unchanged from the guess values due to the penalty method imposed (which removes dependency of $\phi_1$ variables in the separator from the solution). It is to be noted that all reference values for model parameters and constants are adopted from Kumaresan and Zhang. These results obtained for the $\phi_1$ & $\phi_2$ initial distributions are used to initialize the simulations for the full mathematical Li-S battery model.

The simulations carried out, for the initial conditions and all following tests are performed on a spatial grid of 25 points. Although the Python script is generalized to account for as many spatial points, it was decided to test with 25 points for faster computational efficiency, which was also verified to produce considerably good accuracy (to be discussed further in sections 4.3 - 4.5).

## 4.2) 1D Li-S MODEL WITHOUT PRECIPITATION/DISSOLUTION DYNAMICS

To initially verify the capabilities of the solver to simulate the complex 1D set of equations, the full 1D Li-S model was first simplified to not account for the precipitation and dissolution dynamics. The results obtained here provide a good understanding of how the battery system generally performs, and validates the capability of the solver.

The precipitation and dissolution dynamics are set to not play any role through the assumptions made below:

- The pore volume fractions, $\epsilon$ across the separator and cathode are assumed to be constant and homogenous throughout.
- The precipitation/dissolution rates, $R_i$ for the $Li_2S_{(s)}$ & $S_{8(s)}$ species are set to be zero. ($i = Li^+,\ S_{8(l)},\ S^{2-}$)
- $k_k$ the precipitation/dissolution rate constant of $Li_2S_{(s)}$ & $S_{8(s)}$ are also set to be zero.
- Following from $k_k = 0$, $R_k' = 0$, which removes the contributions of equations [10], [14], [15] and [19] from the overall system.

The initial simulations carried out were tested with constant applied currents of 0.5A and 0.05A. The results show instabilities and significantly larger errors for the larger current discharge profiles. This could be attributed to numerical instabilities faced when tuning the solver hyper-parameters and un-modified redundant boundary conditions during initial testing. (Redundancy of BCs arises from flux, $N_i$ & electrolyte current, $i_e$ conditions, since $i_e$ is a function of the flux).

Nevertheless, the results obtained align qualitatively with the expected mechanisms of discharge without precipitation and dissolution dynamics. Note that the results provided here are for pre-tuned solver simulations, with larger errors compared to the finalized results with the full 1D Li-S model with precipitation/dissolution dynamics taken into account. However, the results

obtained here was a huge milestone showing the success of the bespoke solver in simulating the complex system of equations.

The findings obtained are provided in figure 5 below for both 0.5A and 0.05A currents:

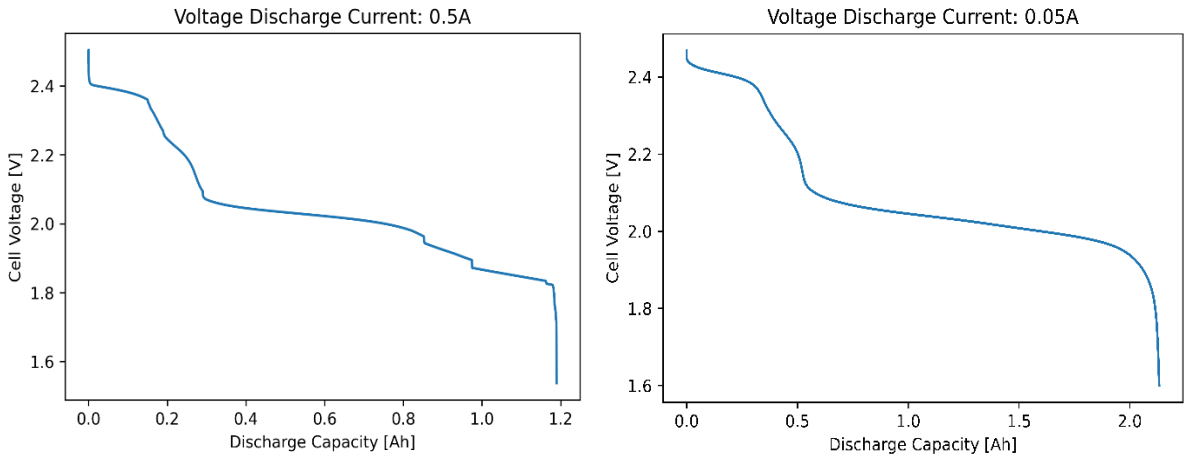


Figure 5. Voltage discharge profiles for 0.5A and 0.05A applied currents.

The discharge profile in figure 5 clearly shows 2 plateau regions, the high plateau and low plateau. The high plateau is attributed to the to the initial reduction of $S_{8(l)}$ species which occurs at a voltage range of between 2.3V-2.4V. The low plateau is characterized by a more stable reduction process of polysulfide species into $S^{2-}$ species, which occurs at a voltage range of 2.0V-2.1V. However, for simulations run without precipitation/dissolution dynamics, the transition region between the high and low plateaus do not exhibit, a 'dip and rise' in voltage, which is attributed to the precipitation of $Li_2S$ and dissolution of $S_{8(s)}$ (will become more apparent in the next section). The end point of discharge is a large drop-off in voltage due to the depletion of higher order polysulfide species which act as the active material for sustaining the voltage plateaus. Note that the overall cell voltage is calculated via $\phi_1|_{x=x_s+x_c} - \phi_2|_{x=0}$.

This is more apparent and clearly observed by plotting the average concentration of species in the cathode with time. The average concentration of polysulfide species in the cathode is formulated using the equation given below:

$$C_{i,avg} = \frac{1}{L_{cath}} \int_{x=x_s}^{x=x_s+x_c} C_i \, dx = \frac{1}{L_{cath}} \sum_{\Delta x} C_i \, . \, \delta x \qquad [39]$$

Where the sum of species concentration is taken over the spatial nodes, $\sum_{\Delta x}*$, of the cathode, with $L_{cath}$ being the length of the cathode region. The results for both 0.5A and 0.05A discharge species time evolution is given in figure 6 below:

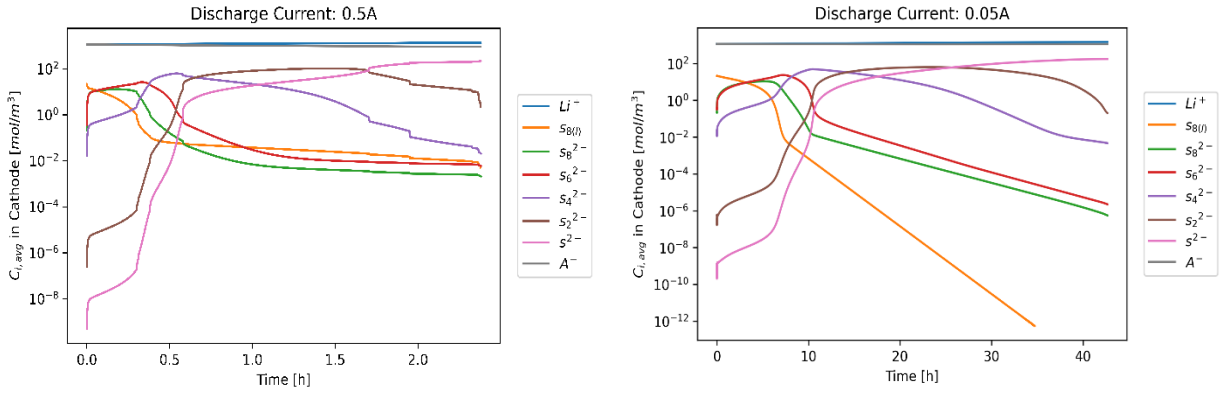


Figure 6. Average species concentrations in the cathode.

It is clearly seen, that the overall concentration of the higher order polysulfides ($S_{8(l)}$, $S_8^{2-}$, $S_6^{2-}$, $S_4^{2-}$) generally decreases over time, while there is an increase in the lower order polysulfides ($S_2^{2-}$, $S^{2-}$). The $Li^+$ species which is assumed to have a large initial concentration (homogenous across the cell initially) does not change much provided there are no precipitation reactions occurring in the cathode. The $A^-$ species also exhibit relatively negligible change in overall concentration as these species do not take part in any redox or electrochemical reactions.

The mass conservation of the $A^-$ species is an imperative metric measurement to quantify the error in the overall system, given these species are non-reactants and only move across the cell via diffusion due to potential and concentration gradients. Also, given the nature of zero precipitation/dissolution of sulfur species, one can also use the mass conservation of sulfur from the transport equations as another error metric (however, this is only the case when there is **NO**

precipitation and dissolution dynamics in the system). The total mass of the anion $A^-$ species in the system is calculated using the formula below:

$$A^-_{total\ mass} = \frac{1}{x_s + x_c} \int_{x=0}^{x=x_s+x_c} \epsilon_p C_{A^-}\ dx = \frac{1}{x_s + x_c} \sum_{\Delta x} \epsilon_p C_{A^-}.\delta x \quad [40]$$

The sum is taken over all spatial nodes of the whole cell domain. Since there is no precipitation and dissolution dynamics and the pore volume fractions of the cathode and separator do not change with time, for this analysis the $\epsilon_p$ term can be omitted. This does not apply to the system involving precipitation and dissolution, which necessitate additional care in calculating the overall $A^-$ mass and require modifications at the boundaries (to be discussed in the next section).

The overall sulfur mass or more precisely the equivalent mass is formulized as below:

$$S_{total\ mass} = \sum_i \left\{ m_i \times \frac{1}{x_s + x_c} \int_{x=0}^{x=x_s+x_c} \epsilon_p C_i\ dx \right\} = \frac{1}{x_s + x_c} \sum_i \left\{ m_i \times \sum_{\Delta x} \epsilon_p C_{A^-}.\delta x \right\} \quad [41]$$

Where $i$ represents all the polysulfide species, and $m_i$ is the number of sulfur molecules in each polysulfide species. The results for both the $A^-$ and total sulfur mass conservation are given in figure 7 below for the different current discharges:

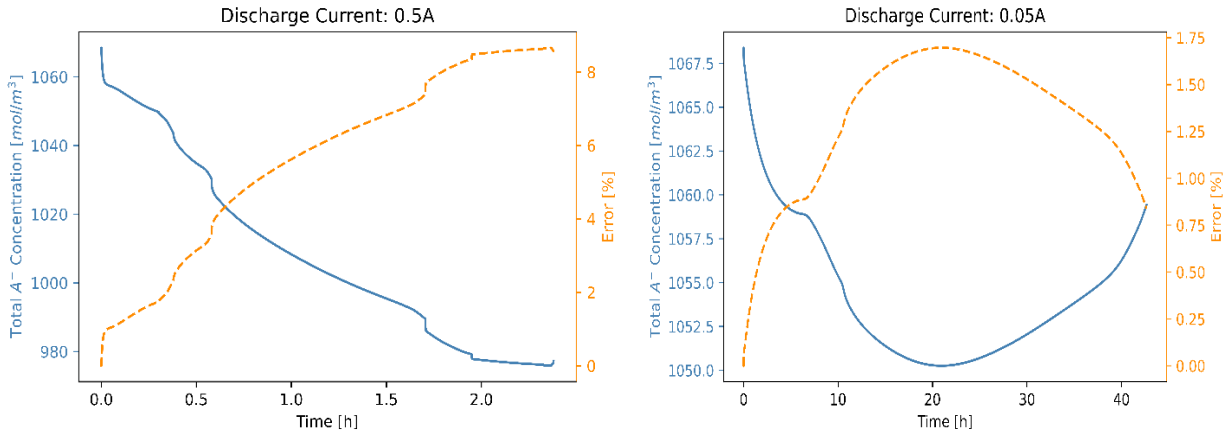


Figure 7. $A^-$ mass conservation plots.

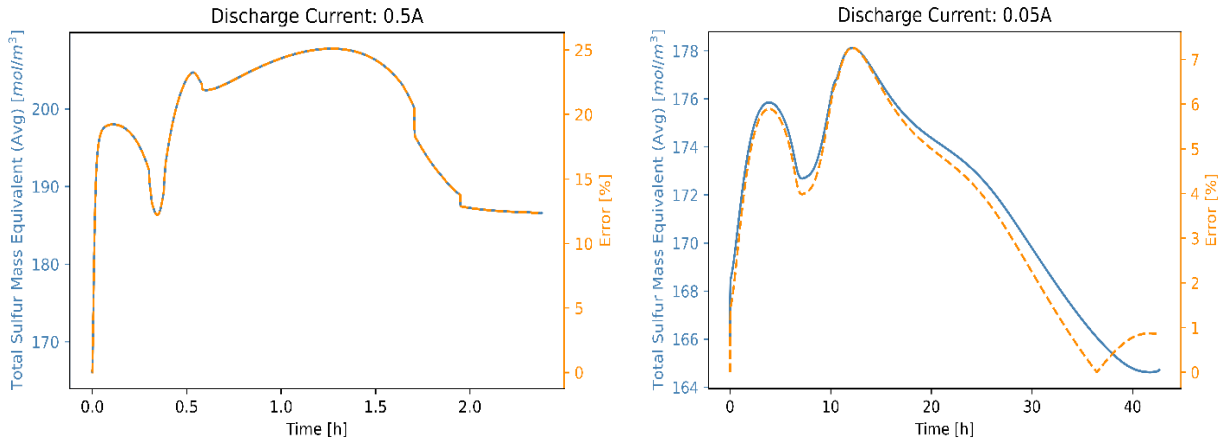


Figure 8. Total sulfur mass conservation plots.

As shown above, the mass conservation errors for the 0.5A discharge is significantly higher than that of the 0.05A. However, as mentioned before, this is likely attributed to initial numerical instabilities experienced by the pre-tuned solver coupled with un-modified boundary conditions. These instabilities are rectified via solver hyper-parameter tuning, and predominantly modifying the prescribed boundary conditions for the full model with precipitation/dissolution implemented (will be discussed about in the next section).

## 4.3) 1D Li-S MODEL WITH PRECIPITATION/DISSOLUTION DYNAMICS

The overall 1D Li-S model is implemented following all the equations detailed in the Methodology section [7-21]. The problem faced during the implementation of the model with precipitation/dissolution dynamics was the influence of the added mechanisms to the original boundary conditions, which lead to many numerical instabilities and overflow errors encountered while running the initial simulations. The original boundary conditions, mainly the conditions underlined in red in figure 2, were modified to the equations given in red. The zero concentration and electrolyte potential gradients at the cathode current collector boundary (similar for potential gradient condition in blue for anode boundary) was adopted from existing Li-Ion battery models as detailed by Wu B (17). The accuracy of modifications of these boundary conditions were studied using the $A^-$ mass conservation metric.

However, as detailed previously, due to the presence of non-constant pore volume fractions $\epsilon_p$ of the cathode and separator regions, the equation [40] is modified as below to account for this using a half control volume approach at the boundaries:

$$A^-_{total\ mass} = \frac{1}{2}\epsilon_{sep}C_{A^-}|_{x=0} + \sum_{x=\delta x}^{x_s-\delta x}\epsilon_{sep}C_{A^-} + \frac{1}{2}\epsilon_{sep}C_{A^-}|_{x=x_s} + \frac{1}{2}\epsilon_{cath}C_{A^-}|_{x=x_s} + \sum_{x=x_s+\delta x}^{x_s+x_c-\delta x}\epsilon_{cath}C_{A^-} + \frac{1}{2}\epsilon_{cath}C_{A^-}|_{x=x_s+x_c} \quad [42]$$

The results obtained for the **red** modified boundary equations are as follows in figure 9:

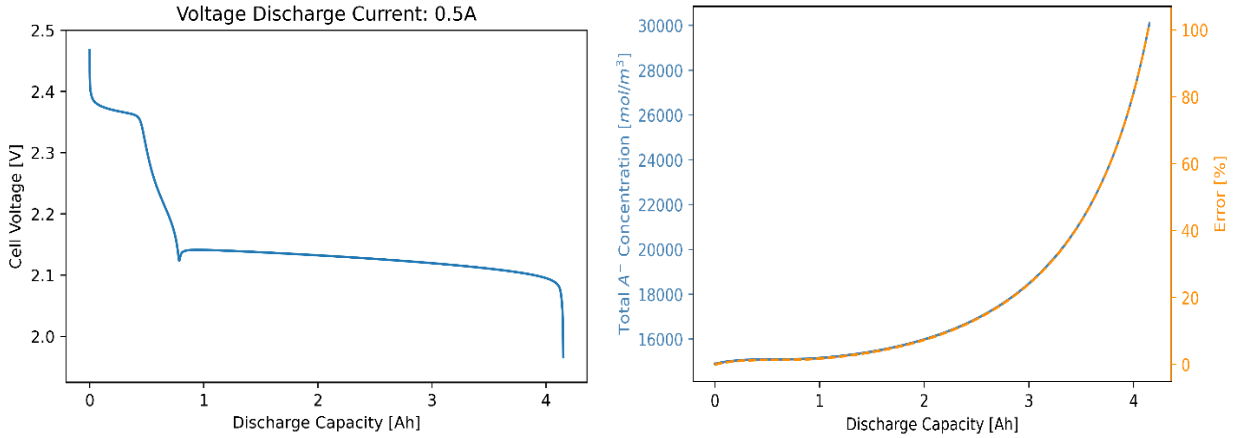


Figure 9. Voltage discharge and $A^-$ mass conservation of red modified boundary conditions.

Evident from above, the voltage discharge profile is qualitatively accurate, however, the mass conservation of $A^-$ shows a worrying increase in error overtime, with a maximum of 100% error. Note since $\delta x$ is a constant, the $\frac{\delta x}{x_s+x_c}$ term in equation [40] is omitted as it is a constant multiple.

To rectify this issue, the boundary conditions are then tested with the conditions given in **blue** as shown in figure 2. Note that there were no changes to the cathode boundary condition given in red, while the separator/cathode interface condition for current continuity was reverted back to the original condition, while a new zero electrolyte potential gradient introduced at the anode (adopted from Li-Ion models as mentioned). The results obtained are in figure 10 below:

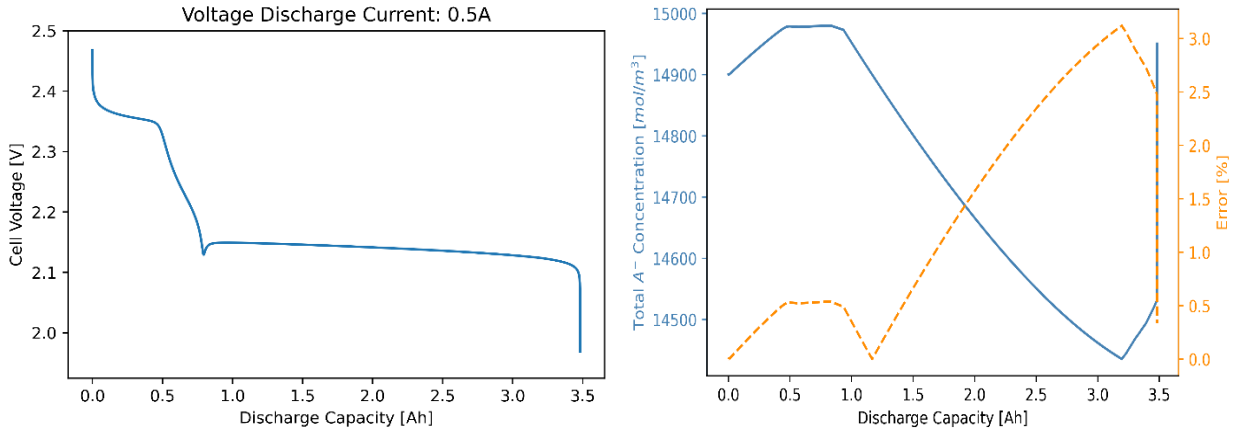


Figure 10. Voltage discharge and $A^-$ mass conservation of blue modified boundary conditions.

With the **blue** boundary conditions (figure 2), it is observed that that mass conservation error for the $A^-$ species is reduced tremendously with only a maximum error of 3%. A slight decrease in overall discharge capacity is observed from the previous red boundary conditions to blue (4Ah to 3.5Ah). These boundary conditions are now employed to further study the model at hand.

The time evolution of species concentration in the cathode is given as such in figure 11:

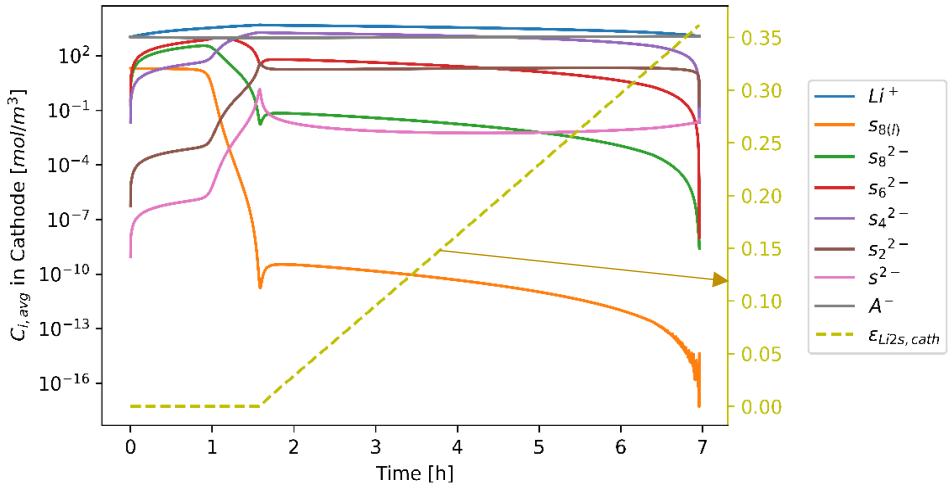


Figure 11. Cathode species time evolution.

From figure 11, it is now evident that the 'dip and rise' during the transition from high to low plateau is attributed to 1) Initial precipitation of $Li_2S_{(s)}$ apparent from the increase of pore volume fraction of $Li_2S_{(s)}$ in the cathode, $\epsilon_{Li2s,cath}$, for which $S^{2-}$ species react with the $Li^+$

causing an overall decrease in the concentrations of polysulfide species, leading to a temporary voltage dip and 2) The dissolution of $S_{8(s)}$ species to account for the decrease of ploysulfide concentrations below the system equilibrium which leads to the rise in voltage.

The results obtained using this new bespoke solver with the assumed simplification provided by Zhang agrees reasonably well with the results provided by Kumaresan in their publication, as shown below in figure 12 (minor differences due to precipitation/dissolution simplifications):

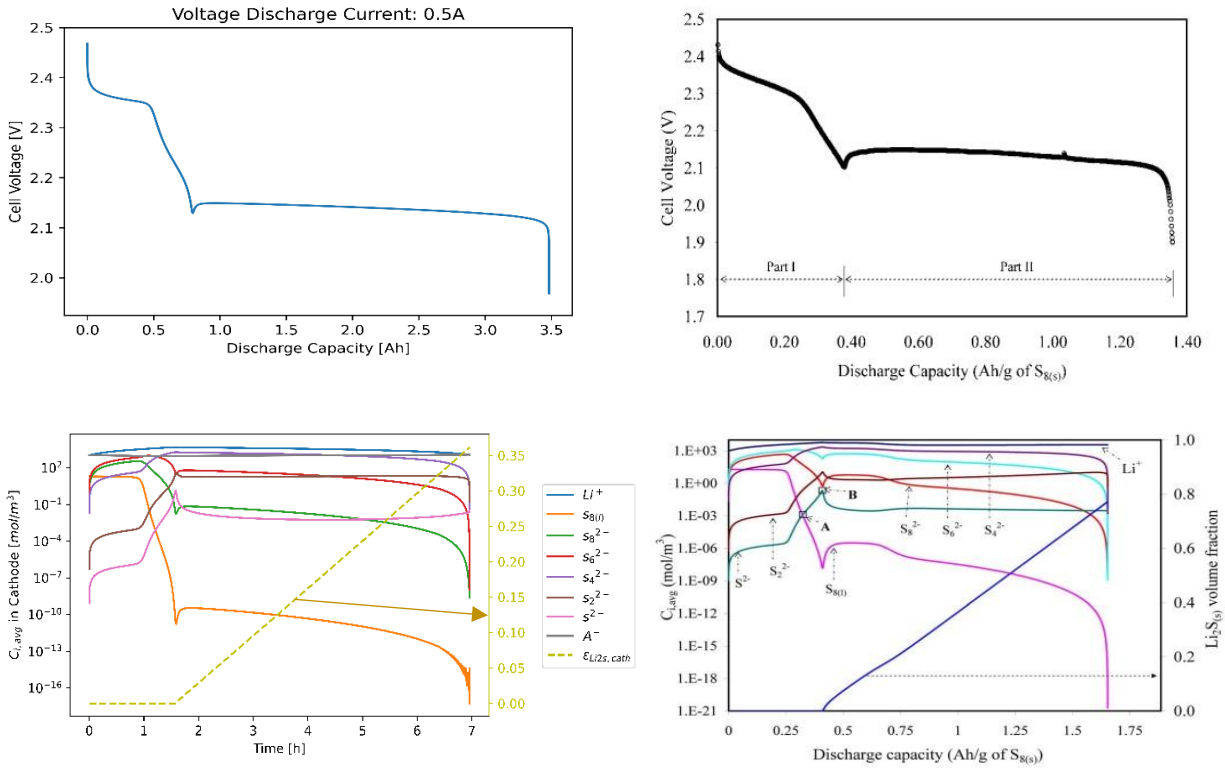


Figure 12. Comparison of plots from Kumaresan and results from novel solver. Experimental, C = 2.5 Ah discharge profile [top right] (6) and species evolution in cathode [bottom right] (6).

Another useful metric in understanding the accuracy of the results obtained is by using the overall cell charge conservation. The charge conservation coupled with species mass conservation form the basis for the derivation of the equations provided describing the 1D Li-S battery model and any other battery model. Hence, further tests are carried out to rectify the charge conservation of the overall results.

From theory, the charge conservation is given as below, where $z_i$ is the ionic charge of species *i* ($i = Li^+, S_{8,l},\ S_8^{2-}, S_6^{2-}, S_4^{2-}, S_2^{2-}, S^{2-}$ & $A^-$ ):

$$\sum_i \epsilon_p z_i C_i = 0 \qquad [43]$$

Applying equation [43] together with the half control volume method employed in equation [42], the overall charge of the cell is evaluated as follows:

$$\sum_i z_i \left[ \frac{1}{2}\epsilon_{sep} C_i|_{x=0} + \sum_{x=\delta x}^{x_s-\delta x} \epsilon_{sep} C_i + \frac{1}{2}\epsilon_{sep} C_i|_{x=x_s} + \frac{1}{2}\epsilon_{cath} C_i|_{x=x_s} + \sum_{x=x_s+\delta x}^{x_s+x_c-\delta x} \epsilon_{cath} C_i + \frac{1}{2}\epsilon_{cath} C_i|_{x=x_s+x_c} \right] \qquad [44]$$

Employing the model from before, the charge conservation of the cell is given in figure 13:

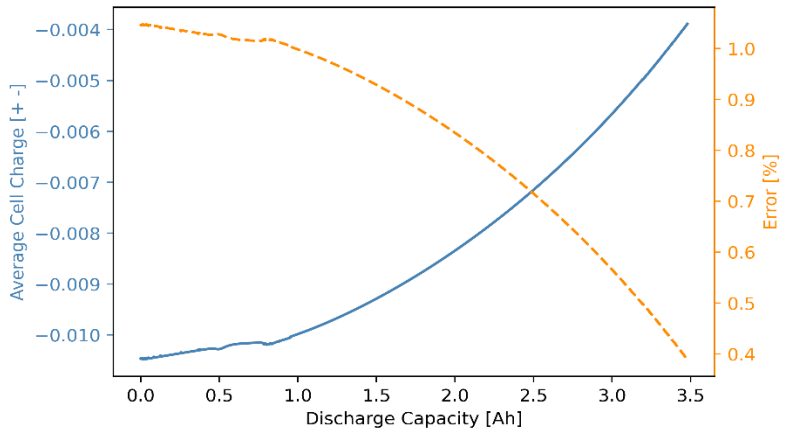


Figure 13. Overall cell charge conservation.

The results, show promising accuracy with the maximum charge conservation error being relatively small at approximately 1%. Note that as mentioned before, all the simulations are carried out on a spatial domain with only 25 grid points, which at first seems too little to accurately capture the intricate spatial changes and gradients that occur within the cell, however is shown to be sufficient with the modestly accurate results obtained.

Another useful metric that is used to study the implications of both the simplification suggested by Zhang and the validity of the results from the solver, is the normalized partial current test suggested by Ghaznavi and Chen (14). The test involves calculating the partial currents in the cathode region of the cell normalized to the applied current, and studying the time evolution of the partial currents and its total sum. The normalized partial currents $I_j^N$ across the cathode is given as:

$$I_j^N = \frac{1}{\frac{I_{App}}{A}} \int_{x=x_s}^{x=x_s+x_c} a_v i_j \, dx = \frac{1}{\frac{I_{App}}{A}} \sum_{\Delta x} a_v i_j \delta x \qquad [45]$$

Where the sum is taken across the cathode spatial nodes. As mentioned by Ghaznavi and Chen (14), the sum of the normalized current should add up to unity by theory, given as:

$$\sum_{j=2}^{6} I_j^N = 1 \qquad [46]$$

The results obtained are depicted in figure 14 below:

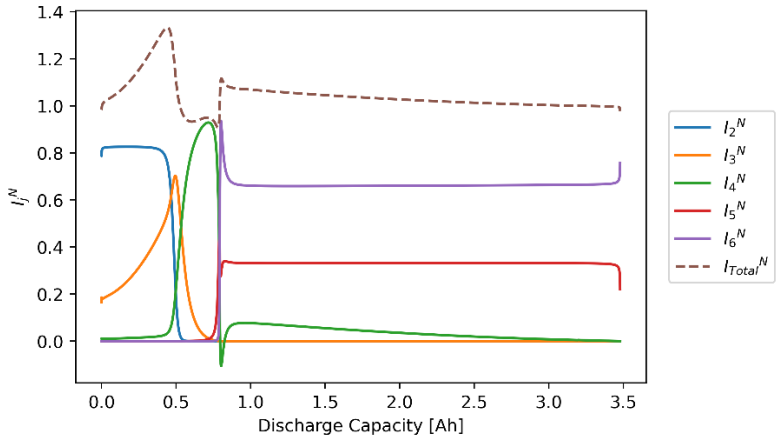


Figure 14. Cathode normalized partial currents time evolution.

It can be seen, at the start of discharge, the sum of the normalized currents seems to increase as opposed to the results provided by Ghaznavi and Chen. The reason to this is not apparent, however is theorized to be due to the initial dissolution of $S_{8(s)}$ species into polysulfide anions

which increases the overall charge density of the cell and acts as a 'source'. The absence of this in the results provided by Ghaznavi and Chen is likely due to the fact that their simulations are carried out using the full Kumaresan model which accounts for precipitation of all polysulfide species, while the results provided here are using the simplification of only accounting for the precipitation of $Li_2S_{(s)}$ species proposed by Zhang. Due to the precipitation of higher-order polysulfides occurring before that of lower-order polysulfides, the precipitation acts as a 'sink' that reduces charge density. This counteracts and balances the initial increase in charge density resulting from the dissolution of $S_{8(s)}$ which is what is observed by Ghaznavi and Chen but not in the simplified model.

The following drop in the sum of the normalized currents which occurs close to the high to low plateau transition, is attributed to a similar reason for which the initial precipitation of $Li_2S_{(s)}$ acts as the 'sink'. The sum of the currents eventually stabilizes and equates to unity as the precipitation/dissolution reactions reach an equilibrium in the low plateau region.

## 4.4) CONSECUTIVE CHARGE TESTS

The solver is also subjected to consecutive charge tests, via either discharge-charge or discharge-rest-charge current profiles. Testing charge from the end-point of the simulations provide valuable information on the overall stability of not only the solver but also the 1D model being studied. The 1D model proposed by Kumaresan, although it is qualitatively a good fit to experimental results, it does have some numerical instabilities, most prominently issues faced during consecutive charge as addressed by Ghaznavi and Chen (10).

The problem faced during consecutive charge, based on the findings of Ghaznavi and Chen were narrowed down to the magnitude of solubility constant of $Li_2S_{(s)}$ species, $K_{Li_2S_{(s)}}$. To verify the findings obtained and to also test the validity of the solver, similar consecutive charge tests were carried out to test this hypothesis. The results obtained are as follows in figure 15:

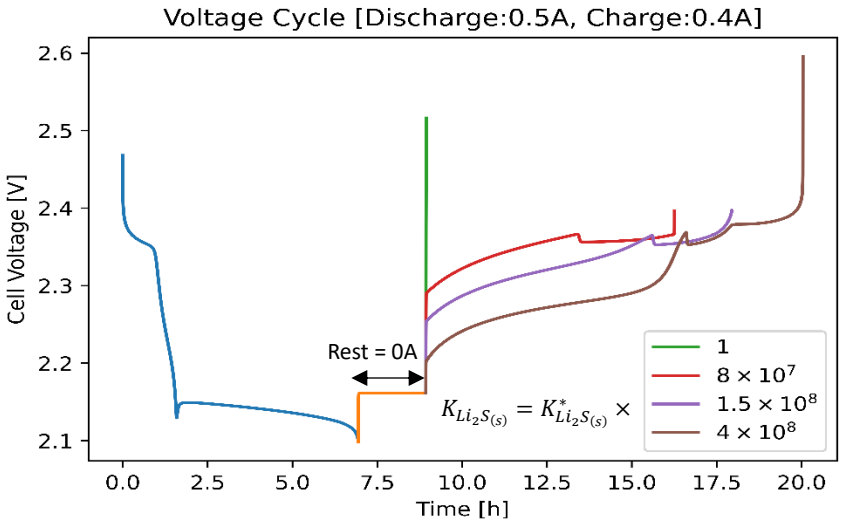


Figure 15. Consecutive charge for varied $K_{Li_2S_{(s)}}$ with discharge-rest-charge current profile.

The plot above clearly shows that for the original value of solubility constant proposed $K^*_{Li_2S_{(s)}} = 9.95 \times 10^{-4} mol/m^3$, the consecutive charge fails almost instantly. Increasing the solubility constant further by multiplying it with larger constants seems to help improve the charge capacity of the model. With a constant multiple of $4 \times 10^8$, the model is capable of fully charging. These findings align well with the results presented by Ghaznavi and Chen, minor differences may be due to the aforementioned simplification adopted in the model presented here.

It was also found that the consecutive charge simulations tend to exhibit instabilities for higher current charges and also initiating the consecutive charge close to the end point of discharge. The latter is due to the widely observed numerical instabilities at the end of discharge that is not only specific to 1D Li-S models but also with simpler 0D models.

Since the solubility constant with the multiple of $4 \times 10^8$ (brown charge curve) is capable of a full charge, the results obtained here were subjected to the $A^-$ mass and overall cell charge conservation tests to further validate these results. The observations for the error metrics tested with the brown charge curve is given as below in figure 16:

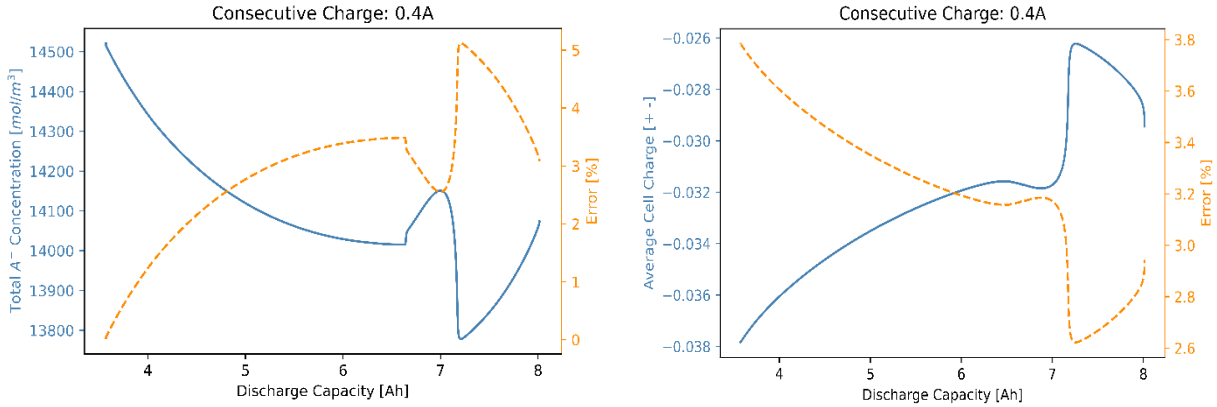


Figure 16. $A^-$ mass & cell charge conservation plots for $K_{Li_2S_{(s)}} = K^*_{Li_2S_{(s)}} \times 4 \times 10^8$.

It can be observed that both the error metrics show reasonably low errors for mass and charge conservation with a maximum error of 5% and 3.8% respectively. However, it was also observed that these errors decrease with charge currents, similar to the observations in section 4.2 for the model without precipitation/dissolution dynamics. Observations are provided in figure 17:

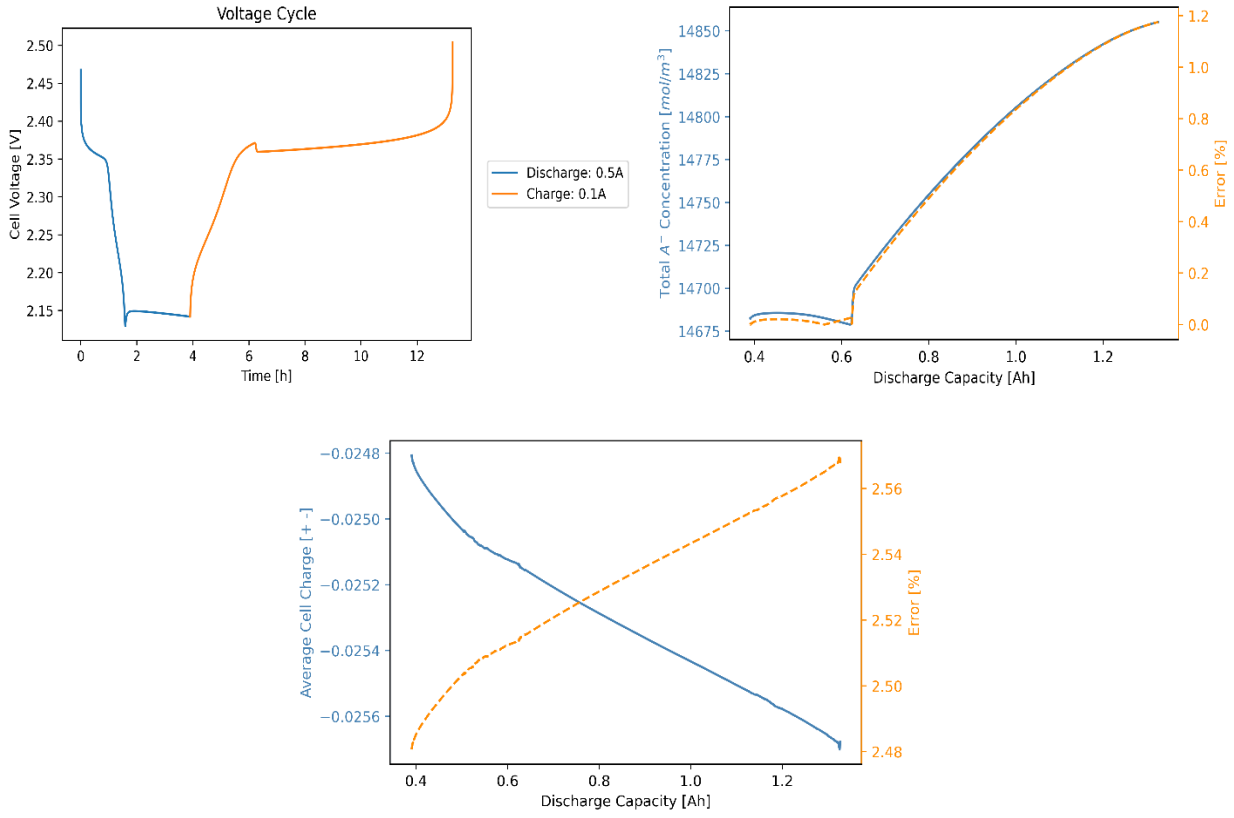


Figure 17. 0.1A consecutive charge profile & respective $A^-$ mass and cell charge conservation.

It is clearly seen that by reducing the charge current from 0.4A to 0.1A, the errors for mass and charge conservation decrease as well to a maximum of 1.2% and 2.6% respectively (most notably for mass conservation). Note that the results provided above is without a rest-phase, however the results for with rest and without rest are relatively similar as the rest-phase is essentially a sub-set of the phase change in applied current to the system going from discharge to charge.

## 4.5) GITT AND NON-CONSTANT CURRENT TESTS

To further validate the capabilities of the solver, the solver is also subjected to a Galvanostatic Intermittent Titration Test (GITT) and non-constant current cycles. These tests are comparable to the consecutive charge tests provided, but also provide a better understanding of the different mechanisms that occur within the 1D model during these current cycles.

The GITT involves passing a square-wave current cycle, with the high-value of the cycle equaling to a constant value (0.5A) and low-value normally being 0A. The other test that was also carried out was to subject the solver and the model to a sinusoidal alternating current and observe the voltage response measured.

These sinusoidal current tests are usually also performed as a basis to Electrochemical Impedance Spectroscopy (EIS). EIS tests are normally conducted experimentally by passing either sinusoidal current or voltage and measuring the response of a cell, which are also sinusoidal in nature. The time series input and output signals of the cell is then transformed into the frequency domain via Fourier Transforms, and is used to calculate the impedance of the cell. The experiment is repeated by varying the frequency of the sinusoidal input, followed by plotting the real and imaginary parts of the impedance for the frequency range on a Nyquist plot. This allows researchers to characterize the different mechanisms that occur within a cell such as diffusion and other electrochemical reactions and their respective operating frequencies.

Although there are some documentations of EIS performed on battery models, it was deemed too time-consuming a task to perform on the current 1D Li-S model as it would require a sweep across a large range of operating frequencies. There also exists the issue of aliasing when dealing with frequency sampling for these numerical solvers due to the adaptive time step method generally used within numerical solvers.

Hence, the results provided here will not be discussed further with regards to the different cell mechanisms operating frequencies, however will solely focus on the error metrics used to assess the validity of the solver. The results obtained for the GITT and sinusoidal current cycles are as below in figure 18:

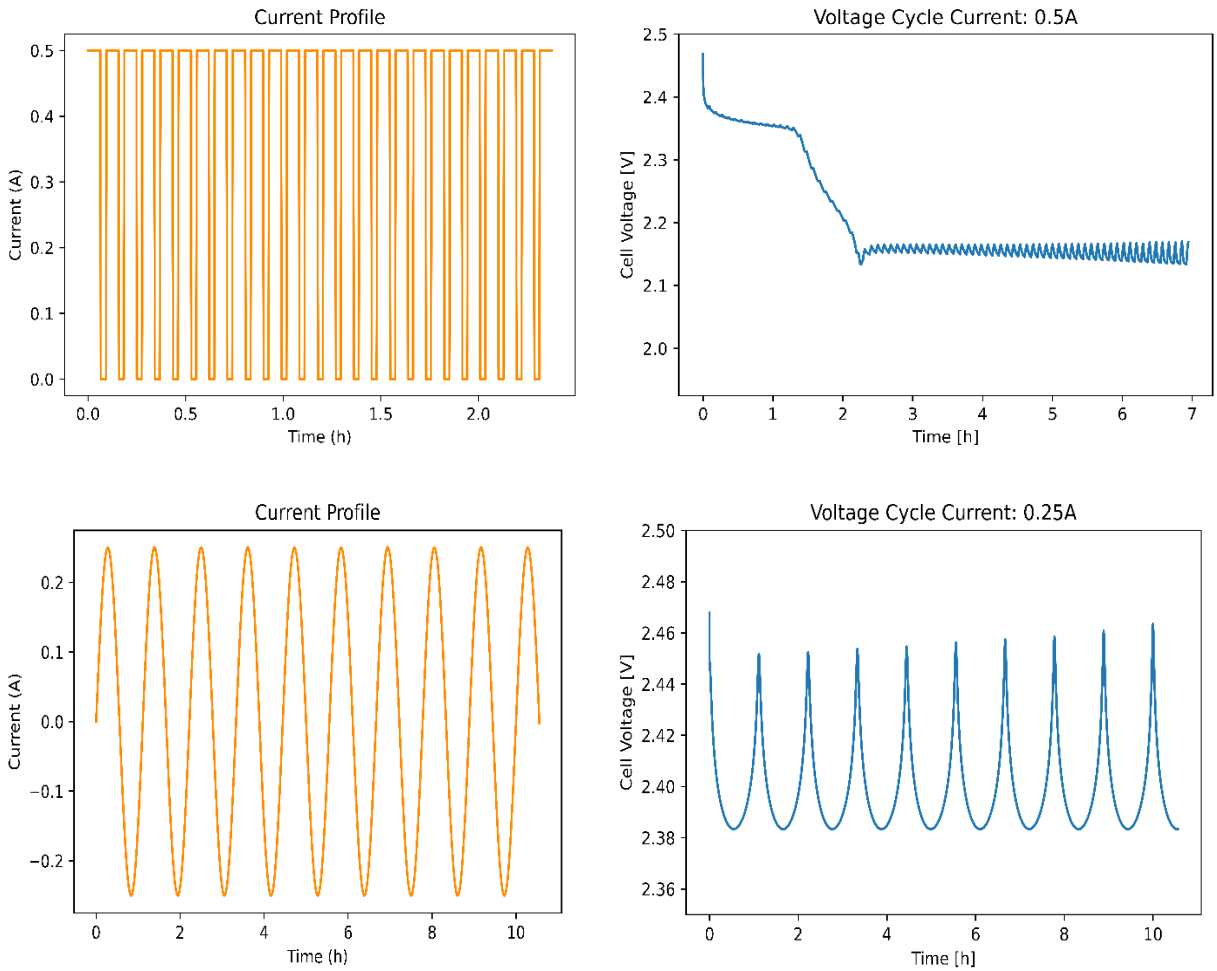


Figure 18. GITT (top) and Sinusoidal current (bottom) cycles.

The results obtained for the GITT cycle shows the effect of the increase in pore volume fraction of the cathode over-time and the diffusion effects that arise from it which are apparent during the later stages of the discharge. The GITT mass and charge conservation errors are comparable to that of a normal discharge which are provided in section 4.3. The mass and charge conservation observations for the sinusoidal current tests are provided in figure 19 below:

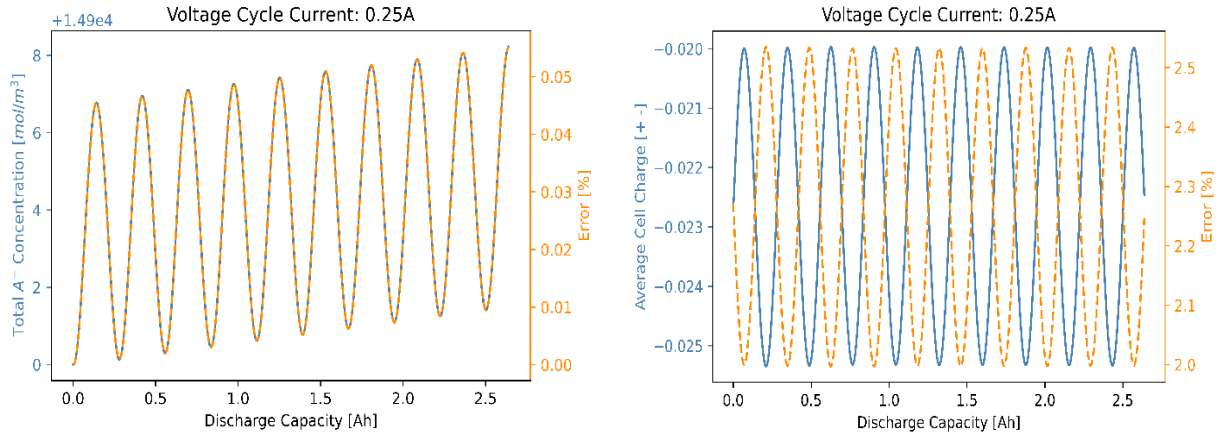


Figure 19. Sinusoidal current cycle $A^-$ mass and overall cell charge conservation plots.

The plots validate the capabilities of the novel solver to simulate a wide range of tests on the implemented 1D Li-S model. With only relatively small mass and charge conservations errors (maximum of 0.06% and 2.5% respectively), it can be concluded that the solver offers promise to simulate more complex 1D models potentially with the application of shuttling effects.

It is also worth mentioning the runtime for most of the simulations carried out are of an average of 10mins per run. This is a huge milestone in efficiency despite the complex nature of spatially resolved models. The shorter runtime for the simulations makes employing high performance computing (HPCs) to parallelize multiple runs a highly efficient and practical approach.

# 5) CONCLUSION

The simulations of the 1D Li-S model, incorporating and excluding precipitation/dissolution dynamics, provided key insights into the system's behavior. Initial discrepancies in the models without these dynamics were attributed to the initial formulation of the boundary conditions. These discrepancies were rectified during the testing phase, leading to more accurate and stable results when the precipitation and dissolution reactions were applied. This underscores the significance of accurate boundary condition formulations in Li-S battery modeling.

Extensive tests on cathode partial currents and species concentration validated the accuracy of the novel solver developed in this research. The normalized partial current test results aligned well with established literature, although some discrepancies were noted during the high-to-low plateau transition, likely due to the simplified assumptions in the current model compared to more complex ones used in other studies. These tests confirm the solver's capability to accurately model the key electrochemical processes in Li-S batteries.

Consecutive charge tests highlighted issues with maintaining numerical stability, particularly concerning the solubility constants of $Li_2S_{(s)}$ species. These challenges echo similar issues found in previous research, emphasizing the need for continued refinement in modeling consecutive charge-discharge cycles to ensure long-term reliability and performance.

The novel solver developed in this study represents a significant advancement in the modeling of Li-S batteries. By effectively incorporating precipitation and dissolution dynamics, it addresses some of the limitations of earlier models, providing a more accurate and stable simulation framework. This research builds on previous studies by refining numerical methods and improving the overall understanding of the complex behaviors within Li-S batteries.

In summary, this work not only rectifies earlier modeling inaccuracies through improved boundary conditions and dynamic mechanisms but also contributes a novel solver that

enhances the precision and reliability of Li-S battery simulations. This positions the research as a valuable continuation and enhancement of the work conducted by other authors in the field.

All the Python scripts that are used for this project can be accessed through the GitHub repository linked below:

https://github.com/Dharshannan/1D_LiS_Battery_Modelling

## 6) ACKNOWLEDGEMENT

I would like to extend my sincere gratitude to my supervisors, Dr. Monica Marinescu and Dr. Michael Cornish, for their invaluable guidance, support, and encouragement throughout the course of this research. Their expertise and insights were instrumental in shaping the direction of this study and in overcoming the numerous challenges encountered along the way. Their dedication to academic excellence and their unwavering commitment to my development as a researcher have been a constant source of inspiration. Thank you for your mentorship, and collaboration. Your contributions have been invaluable, and I am deeply appreciative of the collective effort that has made this research possible.

## REFERENCES

1. Parke CD, Teo L, Schwartz DT, Subramanian VR. Progress on Continuum Modeling of Lithium Sulfur Batteries. *Journal: Sustainable Energy & Fuels.* *https://pubs.rsc.org/en/content/getauthorversionpdf/d1se01090e*.

2. Sulzer V, Marquis SG, Timms R, Robinson M, Chapman SJ. Python Battery Mathematical Modelling (PyBaMM). *Journal of Open Research Software*. 2021;9: 1–8. https://doi.org/10.5334/JORS.309.

3. D. Sugunan. *FUSE_Li-S_Battery_Modelling*. Github; 2023 [Accessed 24th March 2024]. Available from: https://github.com/Dharshannan/FUSE_Li-S_Battery_Modelling.

4. Marinescu M, Zhang T, Offer GJ. A zero dimensional model of lithium-sulfur batteries during charge and discharge. *Physical Chemistry Chemical Physics*. 2016;18(1): 584–593. https://doi.org/10.1039/c5cp05755h.

5. Cornish M, Marinescu M. Toward Rigorous Validation of Li-S Battery Models. *Journal of The Electrochemical Society*. 2022;169(6): 060531. https://doi.org/10.1149/1945-7111/ac7750.

6. Kumaresan K, Mikhaylik Y, White RE. A Mathematical Model for a Lithium–Sulfur Cell. *Journal of The Electrochemical Society*. 2008;155(8): A576. https://doi.org/10.1149/1.2937304.

7. Zhang T, Marinescu M, Walus S, Offer GJ. Modelling transport-limited discharge capacity of lithium-sulfur cells. *Electrochimica Acta*. 2016;219: 502–508. https://doi.org/10.1016/j.electacta.2016.10.032.

8. Mistry A, Mukherjee PP. Precipitation-Microstructure Interactions in the Li-Sulfur Battery Electrode. *Journal of Physical Chemistry C*. 2017;121(47): 26256–26264. https://doi.org/10.1021/acs.jpcc.7b09997.

9. Mikhaylik Y V., Akridge JR. Polysulfide Shuttle Study in the Li/S Battery System. *Journal of The Electrochemical Society*. 2004;151(11): A1969. https://doi.org/10.1149/1.1806394.

10. Ghaznavi M, Chen P. Analysis of a Mathematical Model of Lithium-Sulfur Cells Part III: Electrochemical Reaction Kinetics, Transport Properties and Charging. *Electrochimica Acta*. 2014;137: 575–585. https://doi.org/10.1016/j.electacta.2014.06.033.

11. Marinescu M, O'Neill L, Zhang T, Walus S, Wilson TE, Offer GJ. Irreversible vs Reversible Capacity Fade of Lithium-Sulfur Batteries during Cycling: The Effects of Precipitation and Shuttle. *Journal of The Electrochemical Society*. 2018;165(1): A6107–A6118. https://doi.org/10.1149/2.0171801jes.

12. Hofmann AF, Fronczek DN, Bessler WG. *Mechanistic modeling of polysulfide shuttle and capacity loss in lithium-sulfur batteries*.

13. Yoo K, Song MK, Cairns EJ, Dutta P. Numerical and Experimental Investigation of Performance Characteristics of Lithium/Sulfur Cells. *Electrochimica Acta*. 2016;213: 174–185. https://doi.org/10.1016/j.electacta.2016.07.110.

14. Ghaznavi M, Chen P. Sensitivity analysis of a mathematical model of lithium-sulfur cells part I: Applied discharge current and cathode conductivity. *Journal of Power Sources*. 2014;257: 394–401. https://doi.org/10.1016/j.jpowsour.2013.10.135.

15. Ghaznavi M, Chen P. Sensitivity analysis of a mathematical model of lithium-sulfur cells: Part II: Precipitation reaction kinetics and sulfur content. *Journal of Power Sources*. 2014;257: 402–411. https://doi.org/10.1016/j.jpowsour.2013.12.145.

16. Newhart T. Extension of a Penalty Method for Numerically Solving Extension of a Penalty Method for Numerically Solving Constrained Multibody Dynamic Problems Constrained Multibody Dynamic Problems. https://doi.org/10.25777/381b-8d56.

17. Wu B, Offer GJ, Martinez-Botas R, Brandon NP, Igarashi MH. *Fuel Cell Hybrid Electric Vehicle Powertrain Modelling and Testing*, Ph.D. Thesis, Imperial College London, 2014.